ISSN 1674-1056
http://cpb.iphy.ac.cn
http://iopscience.iop.org/cpb
中国物理 B
Chinese Physics
中国物理 Chinese Physics B

The structural, electronic, and optical properties of organic-inorganic mixed halide perovskites $CH_3NH_3Pb(I_{1-y}X_y)_3$(X=Cl, Br)

Miao Jiang(姜淼), Naihang Deng(邓乃航), Li Wang(王丽), Haiming Xie(谢海明), Yongqing Qiu(仇永清)
Citation: Chin. Phys. B . 2018, 27(6): 067102. **doi:** 10.1088/1674-1056/27/6/067102

Journal homepage: http://cpb.iphy.ac.cn; http://iopscience.iop.org/cpb

What follows is a list of articles you may be interested in

Effect of pressure on the elastic properties and optoelectronic behavior of $Zn_4B_6O_{13}$: First-principles investigation

Pei-Da Wang(王培达), Zhen-Yuan Jia(贾镇源), Yu-Han Zhong(钟玉菡), Hua-Yue Mei(梅华悦), Chun-Mei Li(李春梅), Nan-Pu Cheng(程南璞)
Chin. Phys. B . 2018, 27(5): 057101. **doi:** 10.1088/1674-1056/27/5/057101

Magnetism, optical, and thermoelectric response of $CdFe_2O_4$ by using DFT scheme

Q Mahmood, M Yaseen, K C Bhamu, Asif Mahmood, Y Javed, Shahid M Ramay
Chin. Phys. B . 2018, 27(3): 037103. **doi:** 10.1088/1674-1056/27/3/037103

Structural, electronic, and mechanical properties of cubic TiO_2: A first-principles study

Debashish Dash, Chandan K Pandey, Saurabh Chaudhury, Susanta K Tripathy
Chin. Phys. B . 2018, 27(1): 017102. **doi:** 10.1088/1674-1056/27/1/017102

Tuning electronic properties of the S_2/graphene heterojunction by strains from density functional theory

Jun-Hui Lei(雷军辉), Xiu-Fen Wang(王秀峰), Jian-Guo Lin(林建国)
Chin. Phys. B . 2017, 26(12): 127101. **doi:** 10.1088/1674-1056/26/12/127101

Strain engineering of electronic and magnetic properties of Ga_2S_2 nanoribbons

Bao-Ji Wang(王宝基), Xiao-Hua Li(李晓华), Li-Wei Zhang(张利伟), Guo-Dong Wang(王国东), San-Huang Ke(柯三黄)
Chin. Phys. B . 2017, 26(5): 057102. **doi:** 10.1088/1674-1056/26/5/057102

The structural, electronic, and optical properties of organic–inorganic mixed halide perovskites $CH_3NH_3Pb(I_{1-y}X_y)_3$ (X = Cl, Br)*

Miao Jiang(姜淼)[1], Naihang Deng(邓乃航)[1], Li Wang(王丽)[1], Haiming Xie(谢海明),[1,2] and Yongqing Qiu(仇永清)[1,2,†]

[1] Institute of Functional Material Chemistry, Faculty of Chemistry, Northeast Normal University, Changchun 130024, China
[2] National & Local United Engineering Laboratory for Power Battery, Faculty of Chemistry, Northeast Normal University, Changchun 130024, China

(Received 4 January 2018; revised manuscript received 3 April 2018; published online 10 May 2018)

Methylammmonium lead iodide perovskites ($CH_3NH_3PbI_3$) have received wide attention due to their superior optoelectronic properties. We performed first-principles calculations to investigate the structural, electronic, and optical properties of mixed halide perovskites $CH_3NH_3Pb(I_{1-y}X_y)_3$ (X = Cl, Br; y = 0, 0.33, 0.67). Our results reveal the reduction of the lattice constants and dielectric constants and enhancement of band gaps with increasing doping concentration of Cl^-/Br^- at I^-. Electronic structure calculations indicate that the valance band maximum (VBM) is mainly governed by the halide p orbitals and Pb 6s orbitals, Pb 6p orbitals contribute the conduction band minimum (CBM) and doping does not change the direct semiconductor material. The organic cation $[CH_3NH_3]^+$ does not take part in the formation of the band and only one electron donates to the considered materials. The increasing trends of the band gap with Cl content from $y = 0$ (0.793 eV) to $y = 0.33$ (0.953 eV) then to $y = 0.67$ (1.126 eV). The optical absorption of the considered structures in the visible spectrum range is decreased but after doping the stability of the material is improving.

Keywords: density functional theory, organic–inorganic perovskite, doping, absorption efficiency

PACS: 71.15.Mb, 87.16.A–, 78.20.Ci, 52.25.Mq **DOI:** 10.1088/1674-1056/27/6/067102

1. Introduction

Perovskites have a large family of compounds for the formula of ABX_3 (A = rare-earth, alkali or alkaline earth metal, B = transition metal).[1–3] In the last few years, organic–inorganic hybrid perovskites ABX_3 (A = organic methylamine or formamidinium cation; $B = Pb^{2+}$ or Sn^{2+}; $X = I^-$, Br^- or Cl^-) formula as solar optical absorber materials were firstly reported by Miyasaka *et al.*[4,5] Methylammmonium lead iodide perovskite ($CH_3NH_3PbI_3$), each Pb atom coordinates with six I atoms to form the PbI_6 group.[6] Up to date, the three-dimensional (3D) perovskites structures consist of PbI_6 octahedra play an important role as the superior optical absorbing materials.[7] With the increasing of temperature, the structure of $CH_3NH_3PbI_3$ has a transition from *Pnma* phases (orthorhombic, below 160 K) to $I4/mcm$ (tetragonal) and $Pm3$-m (cubic) phases at 330 K and higher temperature, respectively. The main difference among three phases is the ordering of the noncentrosymmetric $[CH_3NH_3]^+$ cation.[8–13] The efficient solar cell absorbs a wide range spectra from 320 nm to 1000 nm, which are from the visible to near-infrared wavelengths range.[14] The hybrid organic–inorganic perovskites have the power conversion efficiency (PCE) from 3.8% in 2009 to 22.1% in 2016, which are considered as promising materials in the optical field.[15–24] The rapid development progress of $CH_3NH_3PbI_3$ has never been found in other solar cells in history. Organic–inorganic perovskites based on the metal hybrids solar cells have attracted wide photovoltaic research due to its flexibility, easy manufacture, low-cost and high optical absorption efficiency to scientific and industrial applications.[25–36]

For the novel organic–inorganic perovskite materials, many efforts have been devoted to the replacement of A^+, B^{2+}, and X^- by other ions to exploring their outstanding performance.[2,27] The hybrid organic–inorganic perovskites show excellent optical properties in recent experimental measurements and theoretical calculations.[9] The most common strategic choice to the candidates is the Goldschmidt concept, which were proposed by Cheetham and co-workers.[27,37] The ionic tolerance factor (τ) is to assess ionic radius size mismatches the following formed (Eq. (1)),

$$\tau = (r_A + r_X)/\sqrt{2}(r_B + r_X), \tag{1}$$

in which, r_A, r_B, and r_X are the ionic radii of A, B, and X ions, respectively. The values of $0.9 < \tau < 1.0$, the perovskite structure can be obtained; the values of $0.80 < \tau < 0.89$, the perovskite structure distorted to tetragonal or orthorhombic structure; however, for the values of $\tau > 1$, there is a structure transition from 3D to two-dimensional (2D) for perovskites.[25,37]

*Project supported by the Financial Support from the "12th Five-Year" Science and Technology Research Project of the Education Department of Jilin Province (Grant No. [2016] 494) and the National Natural Science Foundation of China (Grant No. 21173035).

†Corresponding author. E-mail: qiuyq466@nenu.edu.cn

© 2018 Chinese Physical Society and IOP Publishing Ltd

According to Goldschmidt's rule and the quantum mechanical consideration, the researchers chose the possible candidates of the periodic table to design related materials. For A site substitution, $MAPbI_3$ has the space group transform from $I4/mcm$ to $P6_3/mmc$ for $DMAPbI_3$ and $TMAPbI_3$ structures (MA = methylammonium, DMA = dimethylammonium, TMA = trimethylammonium), which lead to higher optical band gap from MA to DMA and TMA.[27] For B site substitution, Pb atom was replaced by other group elements such as Ge, Sn, and Ca. Comparing with Pb-based perovskites, Ge-based perovskites have similar absorption spectrum and Sn-based perovskites have lower absorption coefficient.[38,39] The experimental and theoretical results indicate that the calcium-based perovskite has a larger band gap and low mobility, which is not considered as the good optical materials.[2] For X site substitution, $CH_3NH_3PbBr_3$ has larger band gap and lower dielectric function (ε) than $CH_3NH_3PbI_3$, but they do not have a superior optical absorption coefficient than Si and GaAs.[14] For $CH_3NH_3Pb(Br_{1-x}Cl_x)_3$, with the increasing of Cl^- doping leads to an increase of band gap and the decreases of the dielectric constant.[28,29] For $CH_3NH_3Pb(I_{3-x}Br_x)$ (where $0 < x < 10\%$), the overall intensity of the absorption band are decreased.[40] $(CH_3NH_3)Pb(Br_{2.4}Cl_{0.6})$ has the strongest emission intensity and stabilty than the considered perovskite-type counterparts.[41] Up to date, methylammounium (MA) triiodideplumbate and its derivates have been the most widely studied due to their superior performance in optical properties and conductivity for devices. Despite the rapid progress of organic–inorganic perovskite, there are problems that need theoretical investigations. For example, the key mechanism of the effect of ionic substitutions on the physical properties are not fully studied.[42–44]

In the paper, we presented a systematic computational investigation to study the effect arising from chlorine/bromine doping on the structural, electronic and optical properties of the $CH_3NH_3PbI_3$ perovskite based on density functional theory (DFT) calculations. The results indicate that the mixed perovskites have the larger band gap with the Cl^-/Br^- amount increases and has lower optical absorption efficiency compare with the archetypal halide perovskites.

2. Computational method and details

The following *ab initio* structural optimization and electronic properties on $CH_3NH_3Pb(I_{1-y}X_y)_3$ (X = Cl, Br; y = 0, 0.33, 0.67) perovskite structures were calculated by density functional theory (DFT) method with a plane-wave basis set, as implemented in Vienna *Ab initio* Simulation Package (VASP) code.[45,46] The generalized gradient approximation (GGA) parametrized by Perdew–Burke–Ernzerhof (PBE)[47] were adopted for the electron exchange–correlation energy functional. The electron–ion interactions were described by projected-augmented-wave (PAW)[48] pseudopotentials with $1s^1$, $2s^22p^2$, $2s^22p^3$, $6s^26p^2$, $3s^23p^5$, $4s^24p^5$, and $5s^25p^5$ and as valance electrons for H, C, N, Pb, Cl, Br, and I, respectively. All structures have been fully optimized by minimizing atomic forces and stress tensor components via the conjugate gradient algorithm. The Brillouin-zone (BZ) integration[49] has been performed on a Monkhorst–Pack $4 \times 2 \times 4$ k-mesh grid and the plane-wave cutoff is set to 400 eV in all configurations. Calculations were performed with and without spin–orbit coupling. The total electronic energy tolerance is set to 0.1 e^{-4} and the force converge for the structural relaxation is 0.001 eV/Å. The crystal structures were explained by using the VESTA program.[50]

3. Results and discussion

$CH_3NH_3PbI_3$ has the orthorhombic structure in the *Pnma* space group as shown in Fig. 1(a). The fully optimized lattice parameters are $a = 8.437$, $b = 12.813$, and $c = 9.173$ Å, which were in good agreement with experimental values of 8.8362, 12.5804, and 8.5551 Å,[51,52] respectively, indicating the validity of our methodology and pseudopotential in application to the materials. The strong spin–orbit coupling (SOC) effects on reducing the conduction band structures of compounds consisting of heavy elements was studied by Even *et al.*[53] Owing to the large SOC constant of lead atoms, effects of SOC on the band structure of $CH_3NH_3PbI_3$ is huge and cannot be disregarded.[53,54] In Fig. S1 show significant changes of the electronic band structure when accounting for SOC. By comparison we can see that the conduction band is changed by the inclusion of the SOC and the bottom of the conduction band decreases obviously, while the valance band is nearly unaffected. As consequences, the band gap energy is reduced from 1.711 eV to 0.793 eV, which is in line with the results

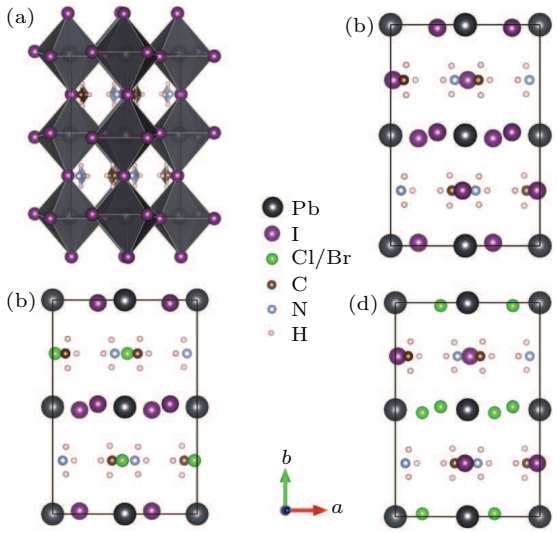


Fig. 1. (color online) (a) The crystal structure of orthorhombic $CH_3NH_3PbI_3$ with PbI_6 octahedral. (b) The $CH_3NH_3PbI_3$ unit cell used for modeling. Panels (c)–(d) display the unique arrangements for $CH_3NH_3Pb(I_{1-y}X_y)_3$ when $y = 0.33$ and $y = 0.67$. Structures visualized with VESTA.

reported by Even *et al.*[53] The valance band maximum (VBM) and the conduction band minimum (CBM) of $CH_3NH_3PbI_3$ are located at the G-point, the results of the direct semiconductor material are in line with the previous reported.[42]

To address the effects of site different substitution concentrations, we consider two kinds of doping fractions of Cl^-/Br^- ($y = 0.33$ and 0.67) within I sublattice (Figs. 1(c)–1(d). The optimized structure parameters, selected interatomic distances of $CH_3NH_3PbI_3$, and mixed halide structures are listed in Table S1 in Appendix A. Because of bigger ionic radius of I^- than Cl^-/Br^-, the partial doping of Cl^-/Br^- with I^- lead to the reduction of lattice constants than pure $CH_3NH_3PbI_3$. The Cl atom has smaller radius compared with Br atom, which leads to a larger change of Pb–Cl distances.

Table 1. Calculated band gap (in unit eV) with and without spin–orbital coupling for $CH_3NH_3Pb(I_{1-y}X_y)_3$ (X = Cl, Br; $y = 0$, 0.33, 0.67) α structures.

	$CH_3NH_3PbI_3$	$CH_3NH_3Pb(I_{0.67}X_{0.33})_3$		$CH_3NH_3Pb(I_{0.33}X_{0.67})_3$	
		X = Br	X = Cl	X = Br	X = Cl
Band gap (without SOC)	1.711	1.844	1.873	1.878	2.094
Band gap (with SOC)	0.793	0.876	0.953	0.989	1.126

The perovskites with mixed halogen anions have different electronic and optical properties than Pb perovskites with pure halogen anions. To further investigate electronic properties of doping and pure $CH_3NH_3PbI_3$, the band structure, total density of states (DOS), and partial density of states (PDOS) for the doping systems of $CH_3NH_3Pb(I_{1-y}X_y)_3$ (X = Cl, Br; $y = 0$, 0.33, 0.67) are calculated. The calculated electronic band structures with and without spin–orbital coupling of the doping phases are shown in Fig. 2 and Figs. S1–S2 in Appendix A. Overall, all the considered configurations have quite similar direct band gaps and both the CBM and VBM were located at the G-point of the Brillouin zone. The bottom of the conduction band is changed by the inclusion of the SOC. As mentioned above, the Pb–Cl distances have changed more than the Pb–Br distance, which leads to Cl-doped perovskites that has a larger band gap than Br-doped perovskites. The band gap increases when iodine is replaced with chlorine/bromine atom, which implies that the absorption coefficients of the Cl/Br doped structure are lower. The result is inconsistent with previous reports that the Br-based structure shows similar trends in increasing of the band gap value with Cl-doped content increases.[29]

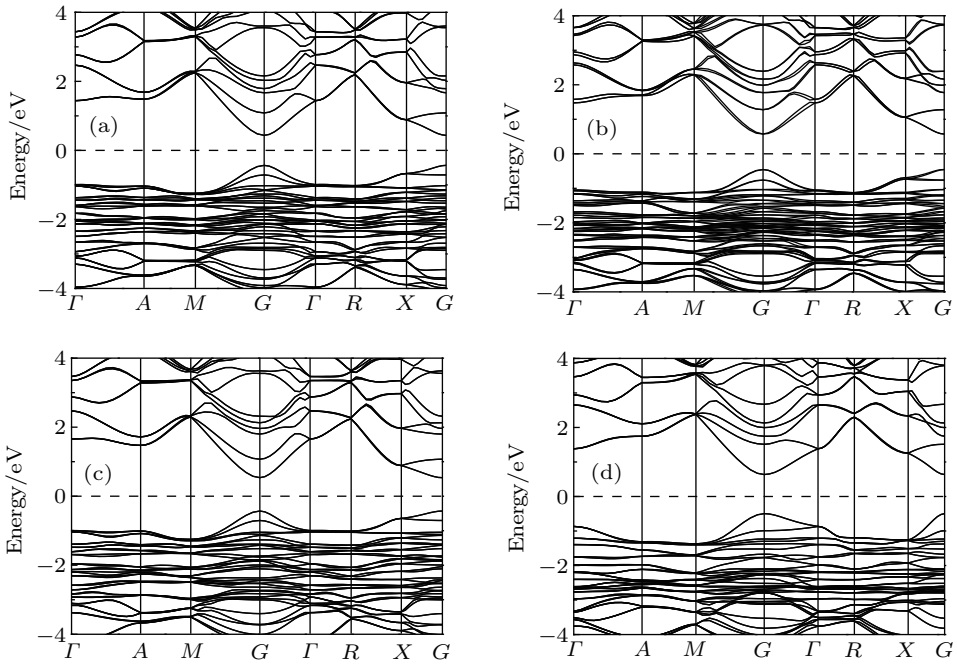


Fig. 2. Electronic band structures of $CH_3NH_3Pb(I_{1-y}Br_y)_3$ with spin–orbital coupling for (a) $y = 0.33$, (b) $y = 0.67$ and $CH_3NH_3Pb(I_{1-y}Cl_y)_3$ for (c) $y = 0.33$, (d) $y = 0.67$. The dashed line indicates the calculated Fermi levels.

From the PDOS of $CH_3NH_3PbI_3$ (Fig. S3), we can see that the VBM is mainly from the mixed contribution from 5p-orbitals of I, 6s-orbitals of Pb, and the CBM is mainly from 6p-orbitals of Pb. From the PDOS of Br-doped systems, as shown in Fig. 3 and Fig. S4, we can see that the addition of Br introduces the 4p-orbitals in the VBM. For $y = 0.33$, the VBM is still mainly 5p-orbitals of I (Fig. 3), mixed contribution from 5p-orbitals of I and 4p-orbitals of Br for $y = 0.67$

(Fig. S4). The p-orbitals of Pb constitute that the CBM remains unchanged. From the PDOS of Cl-doped systems, we can see that Cl-doped and Br-doped systems show the same phenomenon: for y = 0.33, the VBM is still mainly 5p-orbitals of I (Fig. S5), mixed contribution from 5p-orbitals of I and 3p-orbitals of Cl for $y = 0.67$ (Fig. S6). The 6p-orbitals of Pb constitute that the CBM remains unchanged. The $[CH_3NH_3]^+$ consists of organic CH_3 and NH_3 two units, and the calculated PDOS are shown in Fig. 4 and Fig. S7. It is clearly shown that the sharp peaks belong to the strong orbital hybridization between the H 1s and C (N) 2p states, indicating the formation of the C–H and N–H covalent bonds. In conclusion, $[CH_3NH_3]^+$ do not take part in the formation of the band and its major contribution is that it donates one electron to maintain the charge neutrality in materials, which is inconsistent with previously reported.[31] Notable here is that the optical absorption coefficient is related to the electronic structure, which will be discussed in the following.

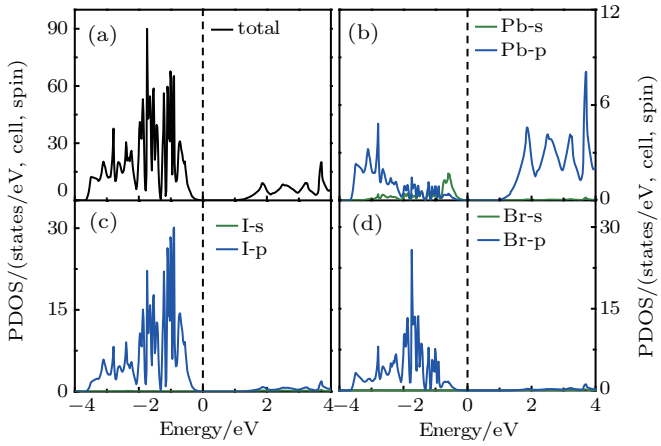


Fig. 3. (color online) Calculated spin-dependent total and partial density of states (PDOS) of $CH_3NH_3Pb(I_{1-y}Br_y)_3$ for $y = 0.33$. The dashed line indicates the calculated Fermi energy.

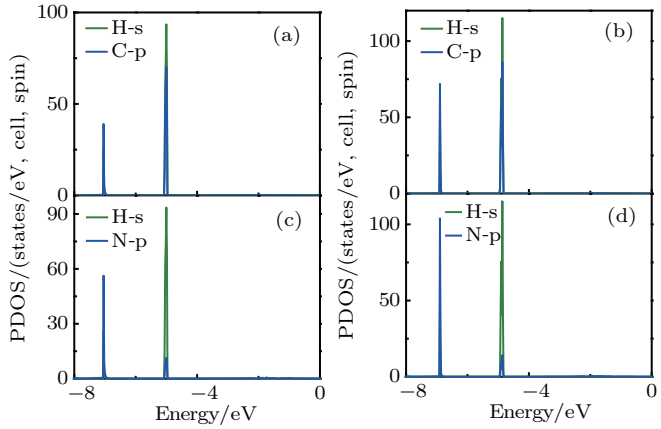


Fig. 4. (color online) Calculated spin-dependent partial density of states (PDOS) of $CH_3NH_3Pb(I_{1-y}Br_y)_3$ for $y = 0.33$ (a) and $y = 0.67$ (b).

The optical properties are important for organic–inorganic compounds, which can discover the potential applications in optoelectronic devices.[55] The linear optical properties can be obtained from the frequency-dependent complex dielectric function $\varepsilon(\omega)$ (Eq. (2)),

$$\varepsilon(\omega) = \varepsilon_1(\omega) + i\varepsilon_2(\omega), \tag{2}$$

where $\varepsilon_1(\omega)$ and $\varepsilon_2(\omega)$ are the real and imaginary parts of the dielectric function. For imaginary part $\varepsilon_2(\omega)$ can be calculated on the basis of Kohn–Sham particle (Eq. (3)) and by applying the Kramers–Kronig relation can obtain the real part $\varepsilon_1(\omega)$.[56]

$$\varepsilon_2(\omega) = \frac{Ve^2}{2\pi\hbar m^2\omega^2}\int \mathrm{d}^3k \sum_{nn'} \left|\langle kn|p|kn'\rangle\right|^2 f(kn) \times (1 - f(kn'))\delta(E_{kn} - E_{kn'} - \hbar\omega). \tag{3}$$

The absorption function $(I(\omega))$ is calculated using Eq. (4).

$$I(\omega) = 2\omega\left(\frac{[\varepsilon_1^2(\omega) + \varepsilon_2^2(\omega)]^{1/2} - \varepsilon_1(\omega)}{2}\right)^{1/2}. \tag{4}$$

The calculated $\varepsilon_1(\omega)$ and $\varepsilon_2(\omega)$ as a function of ω for $CH_3NH_3PbI_3$ are presented in Fig. 5.

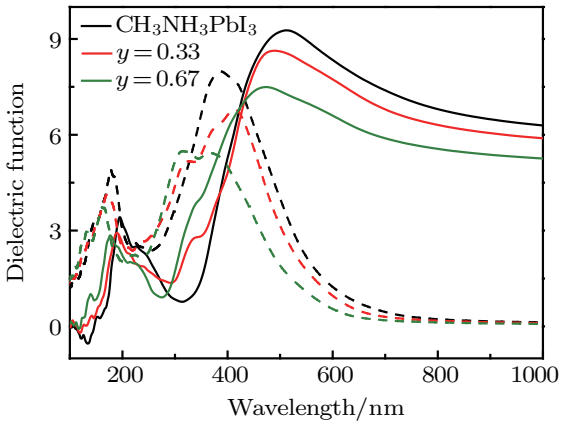


Fig. 5. (color online) Real (solid line) and imaginary (dashed line) parts of the dielectric spectra of $CH_3NH_3Pb(I_{1-y}Br_y)_3$ ($y = 0$, 0.33 and 0.67).

As we can clearly see that the doping compounds have a lower computed imaginary part than pure $CH_3NH_3PbI_3$. The reason for this is that most semiconducting materials have larger band gaps and smaller dielectric constant (Table 1). So, it is not surprising that Cl-doped structure with the band gap of 2.094 eV ($y = 0.67$) has lower dielectric spectra than Br-doped structure with the band gap of 1.878 eV ($y = 0.67$). We also note that, for pure and Br-doped concentration reach to $y = 0.33$, the real part of dielectric function shapes look similar. The phases have positive values in the range of 500 nm to 510 nm. For $y = 0.67$, the dielectric constants are a little from the other considered compounds, which has smaller dielectric constants. Especially for the results shown in Fig. S8, there is an even lower absorber in the visible light spectrum

for Cl-doped reaching to $y = 0.67$. So, the doping compounds are not better absorbers than the pure ones, and Cl-doped have lower absorption coefficients compared with Br-doped systems. We calculated the absorption spectra of the considered compounds to confirm the conclusion. In Fig. 6, we show absorption spectra for $CH_3NH_3Pb(I_{1-y}Br_y)_3$ with $y = 0$, 0.33, and 0.67. As can be seen from Fig. 6, the absorption spectrum of $CH_3NH_3PbI_3$ has a distinct absorption band at 350 nm which is highly consistent with previous theoretical data.[6] We should notice that the absorption coefficient for doping structures are lower than those of $CH_3NH_3PbI_3$. The optical absorption coefficient is related to the electronic structure, for the $Br^-(Cl^-)$ doping system, the band gap is 0.876 eV (0.953 eV) and 0.989 eV (1.126 eV) for $y = 0.33$ and 0.67, which are both higher than $CH_3NH_3PbI_3$ (0.793 eV). So, the overall absorption efficiencies of the doping phases are not superior in comparison with the original $CH_3NH_3PbI_3$ structures in the entire visible spectrum range. The shape of the absorption spectrum becomes narrower as the y value increases. Especially from the calculated Cl-doped absorption coefficient (see Fig. S9), one can see that the absorption coefficients of $y = 0.67$ are concaved downward to negative values in the 320 nm to 460 nm range. Meanwhile, the curve for $CH_3NH_3Pb(I_{0.67}Cl_{0.33})_3$ is narrower in comparison with the pure perovskite.

The Cl-doped structure with the band gap of 1.126 eV ($y = 0.67$) has a lower absorption coefficient than the Br-doped structure with the band gap of 0.989 eV ($y = 0.67$) (see Figs. S8–S9 in Appendix A). Moreover, there is a continuous reduction of the absorption spectrum at longer wavelengths as the Cl^-/Br^- doping concentration increases in the compounds. To address the effects of the different site substitution concentration, we consider another two kinds of doping fractions of Cl^-/Br^- ($y = 0.33$ and 0.67) within the I sublattice (see Fig. S10). For the Br-doped system, when the concentration is up to $y = 0.33$ and $y = 0.67$, we consider two kinds of arrangement for the composition to investigate the effect on electronic conductivity, the unique arrangement for y = 0.33 is shown in Fig. S10, namely α and β.

For the Cl-doped system, we consider the same doping concentration and occupation as the Br-doped system. It is interesting to find that when concentration is up to $y = 0.33$ and $y = 0.67$, we consider two kinds of site occupation, and obtain the same results for site different occupation position: α and β has the lower optical absorption, respectively (see Figs. S11–S12). As in the above mentioned data, there is the same doping concentration, and the different doping occupation has no influences on the optical properties. So, it is clear that the doping phases are not superior to the pure ones in the entire visible light spectrum but after doping the stability of the material is improving.

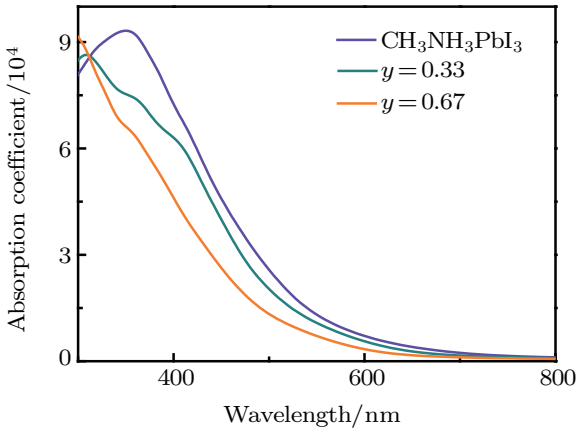


Fig. 6. (color online) The absorption spectra of $CH_3NH_3Pb(I_{1-y}Br_y)_3$ ($y = 0$, 0.33 and 0.67) in the visible light spectrum.

4. Conclusions

In the present paper, a systematic study of the mixed halide $CH_3NH_3Pb(I_{1-y}Cl_y)_3$ and $CH_3NH_3Pb(I_{1-y}Br_y)_3$ perovskites with and without spin–orbit coupling for different y values is carried out by density functional theory calculations. We studied the anionic substitution, which leads to the change of the band gap, density of states, and optical properties of structures. From the calculated band structures and density of states, we can conclude that the considered structures are semiconductors with direct band gaps at the G point and with the increase of doping concentration, the band gap is increased. The band gap is dominated by spin–orbit coupling effects acting mainly on the conduction band. All the considered intensities of the absorption band are decreased, the hybrid perovskites show lower conversion efficiencies than the archetypal halide perovskites. In addition, the Cl-doped structures have smaller lattice distortions and dielectric function in the visible spectrum range in comparison with the Br-doped structures. From the above mentioned results of the high band gap and low absorption efficient, our investigations indicate that Cl/Br-doped perovskites are not good candidates for light materials in solar cells, but after doping the stability of the material improves. The results offer a theoretical foundation for experimental studies of the mixed perovskite and to further explore applications for the other types of materials.

Appendix A: Supporting materials

Some supporting materials for better understanding the present studies are listed and shown in the following tables and figures.

Table S1. Calculated lattice parameters and selected inter-atomic distance (Å) for $CH_3NH_3Pb(I_{1-y}X_y)_3$ (X = Cl, Br; y = 0, 0.33, 0.67) structures.

Orthorhombic halide structures		
	Lattice parameters/Å	Bond and distance/Å
$CH_3NH_3PbI_3$	$a = 8.4384$	Pb–I(1)×2 3.315
	$b = 12.8117$	Pb–I(2)×2 3.215
	$c = 9.1733$	Pb–I(3)×2 3.185
Orthorhombic halide structures		
$CH_3NH_3Pb(I_{0.67}X_{0.33})_3$	Lattice parameters/Å	Bond and distance/Å
X = Br	$a = 8.4413$	Pb–Br(1)×2 3.029
	$b = 11.986$	Pb–I (1)×2 3.205
	$c = 9.237$	Pb–I (2)×2 3.219
X = Cl	$a = 8.4279$	Pb–Cl (1)×2 2.893
	$b = 11.382$	Pb–I (1)×2 3.208
	$c = 9.318$	Pb–I (2)×2 3.227
	Lattice parameters/Å	Bond and distance/Å
X = Br	$a = 8.234$	Pb–I (1)×2 3.178
	$b = 12.550$	Pb–Br(1)×2 3.041
	$c = 8.718$	Pb–Br(2)×2 3.041
X = Cl	$a = 7.863$	Pb- I(1)×2 3.177
	$b = 12.494$	Pb–Cl(1)×2 2.932
	$c = 8.463$	Pb–Cl(2)×2 2.934

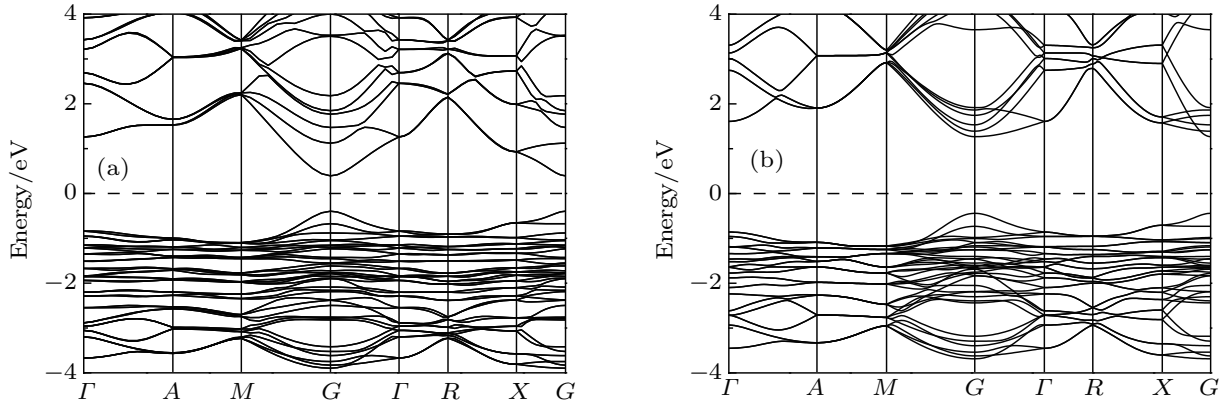
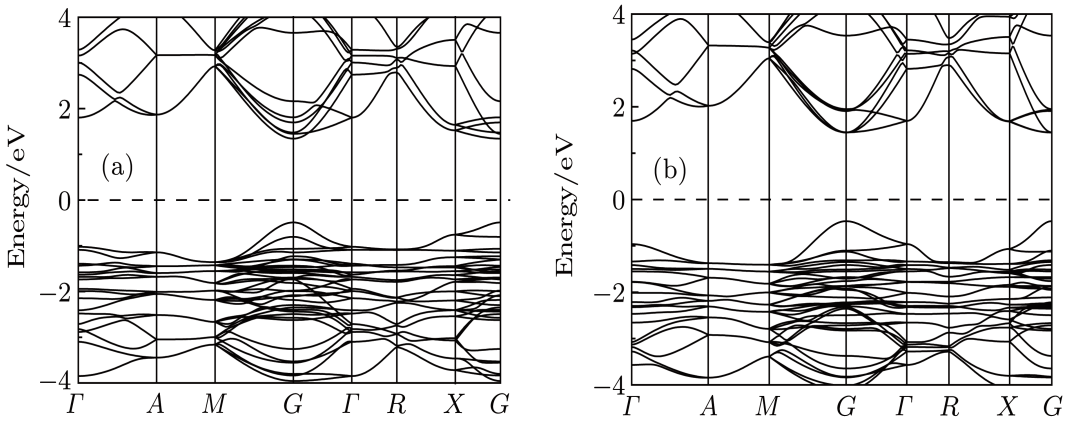


Fig. S1. Electronic band structures of $CH_3NH_3PbI_3$ with (a) and without (b) spin–orbit coupling. The dashed lines indicate the calculated Fermi levels.



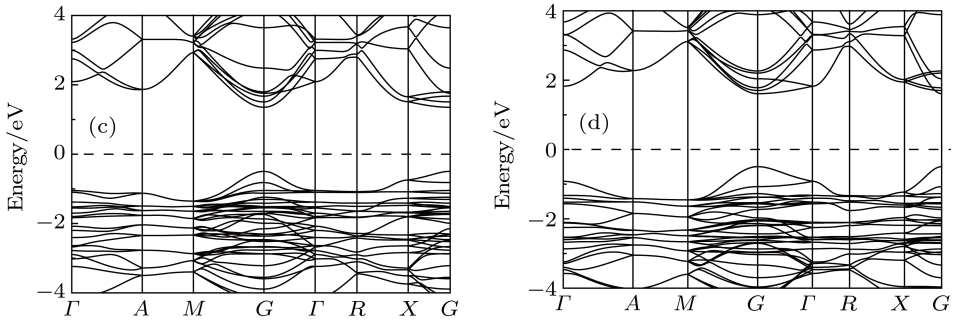


Fig. S2. Electronic band structures of $CH_3NH_3Pb(I_{1-y}Br_y)_3$ without spin–orbit coupling for (a) $y = 0.33$, (b) $y = 0.67$ and $CH_3NH_3Pb(I_{1-y}Cl_y)_3$ for (c) $y = 0.33$, (d) $y = 0.67$. The dashed lines indicate the calculated Fermi levels.

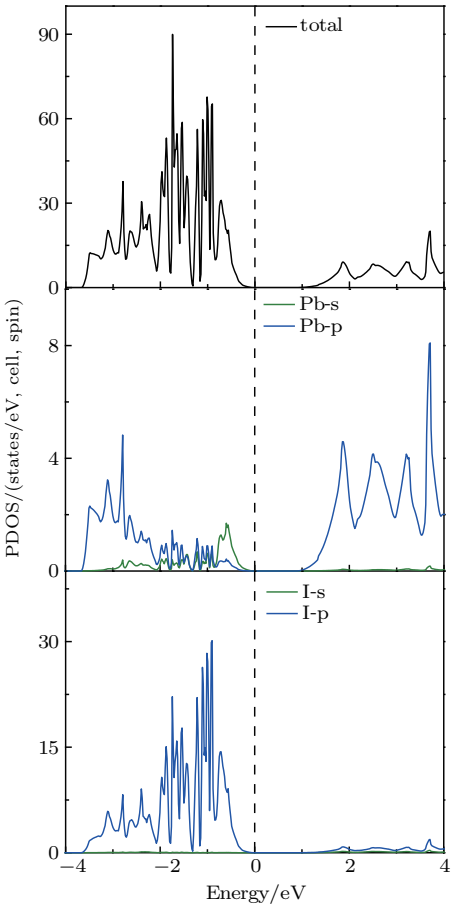


Fig. S3. (color online) Calculated spin-dependent total and partial density of states (PDOS) of $CH_3NH_3PbI_3$. The dashed lines indicate the calculated Fermi energy.

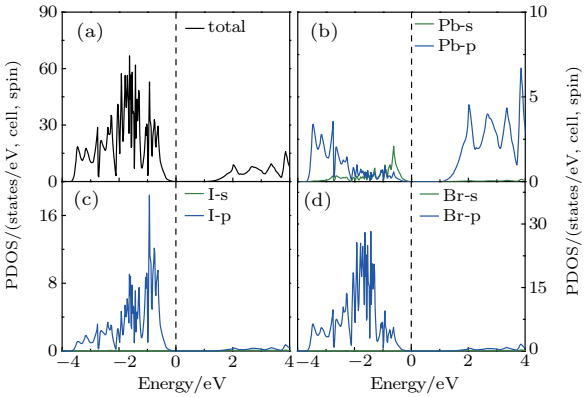


Fig. S4. (color online) Calculated spin-dependent total and partial density of states (PDOS) of $CH_3NH_3Pb(I_{1-y}Br_y)_3$ for $y = 0.67$. The dashed line indicates the calculated Fermi energy.

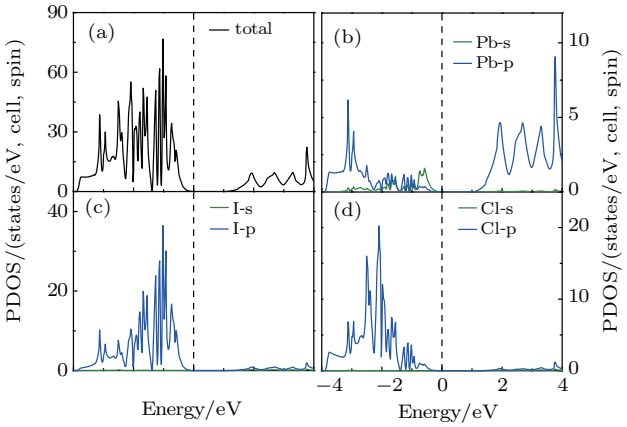


Fig. S5. (color online) Calculated spin-dependent total and partial density of states (PDOS) of $CH_3NH_3Pb(I_{1-y}Cl_y)_3$ for $y = 0.33$. The dashed line indicates the calculated Fermi energy.

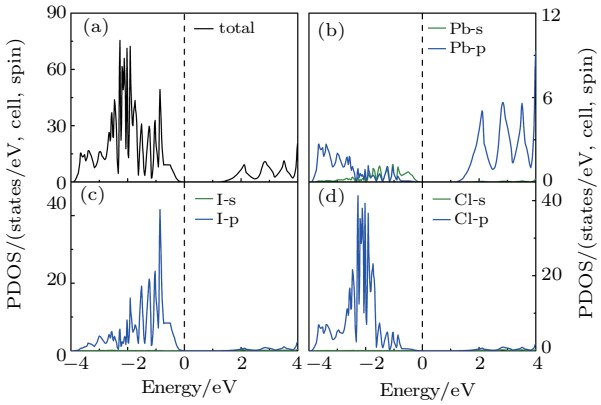


Fig. S6. (color online) Calculated spin-dependent total and partial density of states (PDOS) of $CH_3NH_3Pb(I_{1-y}Cl_y)_3$ for $y = 0.67$. The dashed line indicates the calculated Fermi energy.

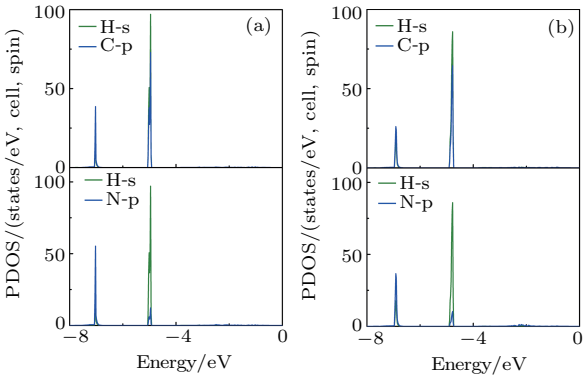


Fig. S7. (color online) Calculated spin-dependent partial density of states (PDOS) of $CH_3NH_3Pb(I_{1-y}Cl_y)_3$ for $y = 0.33$ (a) and $y = 0.67$ (b).

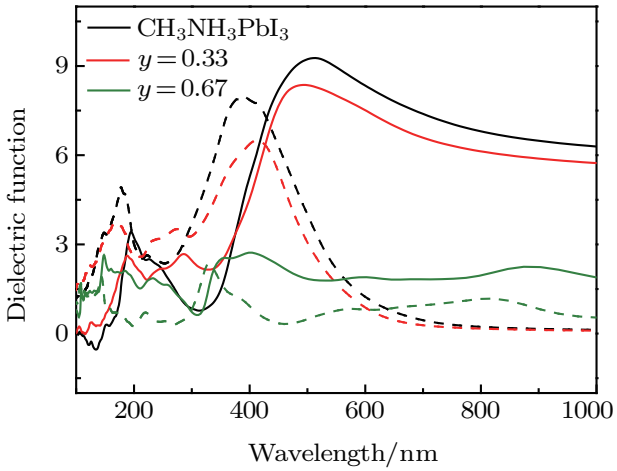


Fig. S8. (color online) Real (solid line) and imaginary (dashed line) parts of the dielectric spectra of $CH_3NH_3Pb(I_{1-y}Cl_y)_3$ ($y = 0$, 0.33, and 0.67).

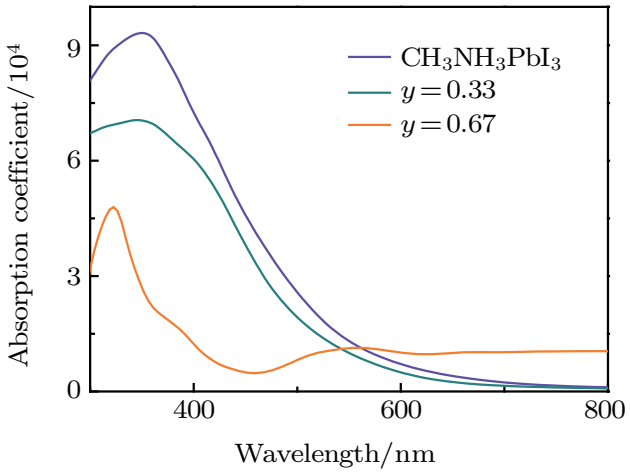


Fig. S9. (color online) The absorption spectra of $CH_3NH_3Pb(I_{1-y}Cl_y)_3$ ($y = 0$, 0.33, and 0.67) in the visible light spectrum.

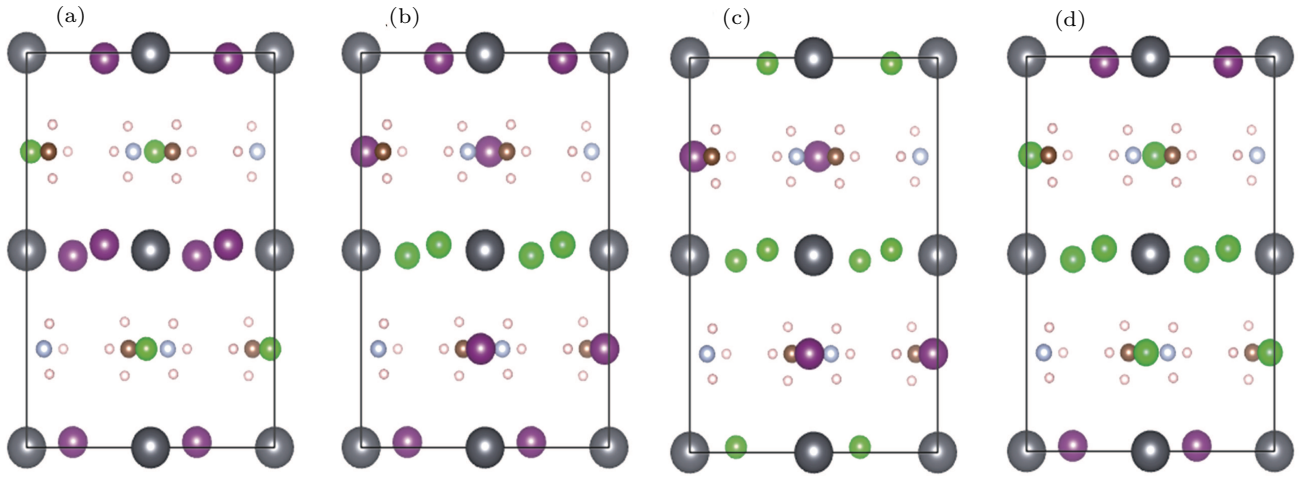


Fig. S10. (color online) Panels (a)–(d) display the unique arrangements for $CH_3NH_3Pb(I_{1-y}X_y)_3$. Panels (a)–(b) display the structure for two kinds of atom configuration when $y = 0.33$, namely α and β. Panels (c)–(d) display the structure for two kinds of atom configuration when $y = 0.67$, namely α and β. Structures visualized with VESTA.

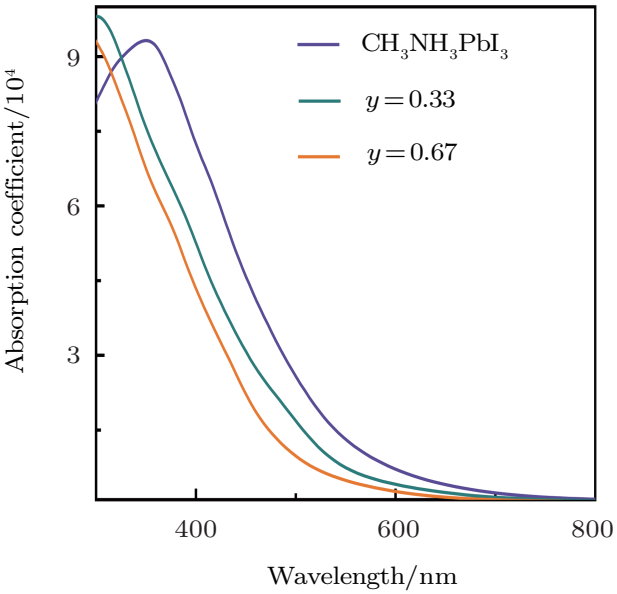


Fig. S11. (color online) The absorption spectra of $CH_3NH_3Pb(I_{1-y}Br_y)_3$ ($y = 0$, 0.33, and 0.67) for β structure in the visible light spectrum.

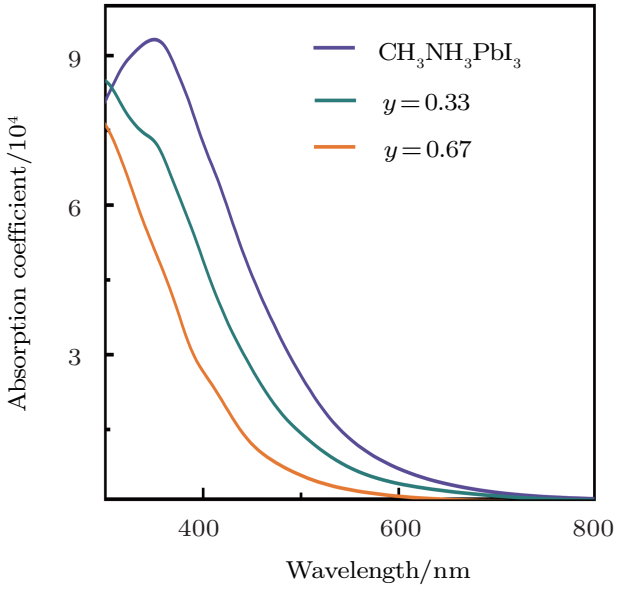


Fig. S12. (color online) The absorption spectra of $CH_3NH_3Pb(I_{1-y}Cl_y)_3$ ($y = 0$, 0.33, and 0.67) for β structure in the visible light spectrum.

Table S2. The atomic coordinates of H, C, N, I, and Pb elements in $CH_3NH_3PbI_3$ structure.

			x	*y*	*z*	Wyckoff position
1	H	H1	0.39555	0.31826	0.38481	8*d*
2	H	H2	0.59173	0.31400	0.58186	8*d*
3	H	H3	0.10445	–0.31826	0.88481	8*d*
4	H	H4	–0.09173	–0.31400	1.08186	8*d*
5	H	H5	–0.39555	0.81826	–0.38481	8*d*
6	H	H6	–0.59173	0.81400	–0.58186	8*d*
7	H	H7	0.89555	0.18174	0.11519	8*d*
8	H	H8	1.09173	0.18560	–0.08186	8*d*
9	H	H9	–0.39555	–0.31826	–0.38481	8*d*
10	H	H10	–0.59173	–0.31400	–0.58186	8*d*
11	H	H11	0.89555	0.31826	0.11519	8*d*
12	H	H12	1.09073	0.31400	–0.08186	8*d*
13	H	H13	0.39555	0.18174	0.38481	8*d*
14	H	H14	0.59173	0.18560	0.58186	8*d*
15	H	H15	0.10445	0.81826	0.88481	8*d*
16	H	H16	–0.09173	0.81400	1.08186	8*d*
17	H	H17	0.33406	0.25000	0.55344	8*d*
18	H	H18	0.64777	0.25000	0.42545	4*c*
19	H	H19	0.16594	–0.25000	1.05344	4*c*
20	H	H20	–0.14777	–0.25000	0.92545	4*c*
21	H	H21	–0.33406	0.75000	–0.55344	4*c*
22	H	H22	–0.64777	0.75000	–0.42545	4*c*
23	H	H23	0.83406	0.25000	–0.05344	4*c*
24	H	H24	1.14777	0.25000	0.07455	4*c*
25	C	C25	0.91185	0.25000	0.04446	4*c*
26	C	C26	–0.41185	–0.25000	0.54446	4*c*
27	C	C27	–0.91185	0.75000	–0.04446	4*c*
28	C	C28	1.41185	0.25000	0.45554	4*c*
29	N	N29	0.93049	0.75000	0.01491	4*c*
30	N	N30	–0.43049	–0.75000	0.51491	4*c*
31	N	N31	–0.93049	1.25000	–0.01491	4*c*
32	N	N32	1.43049	–0.25000	0.48509	4*c*
33	I	I33	0.1865	0.01383	0.18556	8*d*
34	I	I34	0.31350	–0.01383	0.68556	8*d*
35	I	I35	–0.18650	0.51383	–0.18556	8*d*
36	I	I36	0.68650	0.48617	0.31444	8*d*
37	I	I37	–0.18650	–0.01383	–0.18556	8*d*
38	I	I38	0.68650	0.01383	0.31444	8*d*
39	I	I39	0.18650	0.48617	0.18556	8*d*
40	I	I40	0.31350	0.51383	0.68556	8*d*
41	I	I41	0.48258	0.25000	–0.05115	4*c*
42	I	I42	0.01742	–0.25000	0.44885	4*c*
43	I	I43	–0.48258	0.75000	0.5115	4*c*
44	I	I44	0.98258	0.25000	0.55115	4*c*
45	Pb	Pb45	0.50000	0.00000	0.00000	4*b*
46	Pb	Pb46	0.00000	0.00000	0.50000	4*b*
47	Pb	Pb47	–0.50000	0.50000	0.00000	4*b*
48	Pb	Pb48	1.00000	0.50000	0.50000	4*b*

References

[1] Jiang M, Deng N H and Qiu Y Q 2016 *Comput. Theor. Chem.* **1095** 112

[2] Uribe J I, Ramirez D, Osorio-Guillén J M, Osorio J and Jaramillo F 2016 *J. Phys. Chem. C* **120** 16393

[3] Qian J Y, Xu B and Wen W J 2016 *Org. Electron.* **37** 61

[4] Slotcavage D J, Karunadasa H I and McGehee M D 2016 *ACS Energy Lett.* **1** 1199

[5] Brivio F, Caetano C and Walsh A 2016 *J. Phys. Chem. Lett.* **7** 1083

[6] Geng W, Zhang L, Zhang Y N, Lau W M and Liu L M 2014 *J. Phys. Chem. C* **118** 19565

[7] Hong F, Saparov B, Meng W W, Xiao Z W, Mitzi D B and Yan Y F 2016 *J. Phys. Chem. C* **120** 6435

[8] Bechtel J S, Seshadri R and Van der Ven A 2016 *J. Phys. Chem. C* **120** 12403

[9] Yan W L, Lu G H and Liu F 2016 *J. Phys. Chem. C* **120** 17972

[10] Poglitsch A and Weber D 1987 *J. Chem. Phys.* **87** 6373

[11] Ong K P, Goh T W, Xu Q and Huan A 2015 *J. Phys. Chem. Lett.* **6** 681

[12] Nandi P, Giri C, Joseph B, Rath S, Manju U and Topwal D 2016 *J. Phys. Chem. A* **120** 9732
[13] Carignano M A, Kachmar A and Hutter J 2015 *J. Phys. Chem. C* **119** 8991
[14] Feng J and Xiao B 2014 *J. Phys. Chem. Lett.* **5** 1278
[15] Zheng F, Takenaka H, Wang F G, Koocher N Z and Rappe A M 2015 *J. Phys. Chem. Lett.* **6** 31
[16] Sadhanala A, Deschler F, Thomas T H, Dutton S E, Goedel K C, Hanusch F C, Lai M L, Steiner U, Bein T, Docampo P, Cahen D and Friend R H 2014 *J. Phys. Chem. Lett.* **5** 2501
[17] Montero-Alejo A L, Menéndez-Proupin E, Hidalgo-Rojas D, Palacios P, Wahnón P and Conesa J C 2016 *J. Phys. Chem. C* **120** 7976
[18] Filip M R, Verdi C and Giustino F 2015 *J. Phys. Chem. C* **119** 25209
[19] Quarti C, Mosconi E, Umari P and De Angelis F 2017 *Inorg. Chem.* **56** 74
[20] Zhao X G, Yang J H, Fu Y H, Yang D W, Xu Q L and Yu L P 2017 *J. Am. Chem. Soc.* **139** 2630
[21] He J G, Franchini C and Rondinelli J M 2017 *Chem. Mater.* **29** 2445
[22] Wang J F, Fu X N and Wang J T 2017 *Chin. Phys. B* **26** 106301
[23] Qian J Y, Guo Q, Liu L J, Xu B and Tian W J 2017 *J. Mater. Chem. A* **5** 16786
[24] Zhang Y Y, Chen S Y, Xu P, Xiang H J, Gong X G, Walsh A and Wei S H 2018 *Chin. Phys. Lett.* **35** 036104
[25] Dang Y Y, Zhong C, Zhang G D, Ju D X, Wang L, Xia S Q, Xia H B and Tao X T 2016 *Chem. Mater.* **28** 6968
[26] Kuang C Y, Tang G, Jiu T G, Yang H, Liu H B, Li B R, Luo W N, Li X D, Zhang W J, Lu F S, Fang J F and Li Y L 2015 *Nano Lett.* **15** 2756
[27] Mancini A, Quadrelli P, Amoroso G, Milanese C, Boiocchi M, Sironi A, Patrini M, Guizzetti G and Malavasi L 2016 *J. Solid State Chem.* **240** 55
[28] Park J S, Choi S, Yan Y, Yang Y, Luther J M, Wei S H, Parilla P and Zhu K 2015 *J. Phys. Chem. Lett.* **6** 4304
[29] Kumawat N K, Tripathi M N, Waghmare U and Kabra D 2016 *J. Phys. Chem. A* **120** 3917
[30] Stroppa A, Quarti C, De Angelis F and Picozzi S 2015 *J. Phys. Chem. Lett.* **6** 2223
[31] Bernal C and Yang K S 2014 *J. Phys. Chem. C* **118** 24383
[32] Tan Z K, Moghaddam R S, Lai M L, Docampo P, Higler R, Deschler F, Price M, Sadhanala A, Pazos L M, Credgington D, Hanusch F, Bein T, Snaith H J and Friend R H 2014 *Nat. Nanotechnol.* **9** 687
[33] Xiao L, Xu J, Luan J C, Zhang B, Tan Z A and Yao J X 2017 *Org. Electron.* **50** 33
[34] Wu L J, Zhao Y Q, Chen C W, Wang L Z, Liu B and Cai M Q 2016 *Chin. Phys. B* **25** 107202
[35] Sun P, Yu W W, Pan X H, Wei W, Sun Y, Yuan N Y, Ding J N, Zhao W C, Chen X and Dai N 2017 *Chin. Phys. Lett.* **34** 096801
[36] Yan H J, Ku Z L, Hu X F, Zhao W Y, Zhong M J, Zhu Q B, Lin X, Jin Z M and Ma G H 2018 *Chin. Phys. Lett.* **35** 028401
[37] Jacobsson T J, Pazoki M, Hagfeldt A and Edvinsson T 2015 *J. Phys. Chem. C* **119** 25673
[38] Mancini A, Quadrelli P, Milanese C, Patrini M, Guizzetti G and Malavasi L 2015 *Inorg. Chem.* **54** 8893
[39] He Y P and Galli G 2017 *Chem. Mater.* **29** 682
[40] Dar M I, Abdi-Jalebi M, Arora N, Moehl T, Grätzel M and Nazeeruddin M K 2015 *Adv. Mater.* **27** 7221
[41] Zhang M, Yu H, Lyu M Q, Wang Q, Yun J H and Wang L Z 2014 *Chem. Commun.* **50** 11727
[42] Mosconi E, Amat A, Nazeeruddin M K, Grätzel M and Angelis F D 2013 *J. Phys. Chem. C* **117** 13902
[43] Noh J H, Im S H, Heo J H, Mandal T N and Seok S I 2013 *Nano Lett.* **13** 1764
[44] Baikie T, Fang Y A, Kadro J M, Schreyer M, Wei F X, Mhaisalkar S G, Graetzel M and White T J 2013 *J. Mater. Chem. A* **1** 5628
[45] Kresse G and Furthmüller J 1996 *Phys. Rev. B* **54** 11169
[46] Kresse G and Furthmuller J 1996 *Comput. Mater. Sci.* **6** 15
[47] Perdew J P, Burke K and Ernzerhof M 1996 *Phys. Rev. Lett.* **77** 3865
[48] Blöchl P E 1994 *Phys. Rev. B* **50** 17953
[49] Blöchl P E, Jepsen O and Andersen O K 1994 *Phys. Rev. B* **49** 16223
[50] Momma K and Izumi F 2008 *J. Appl. Cryst.* **41** 653
[51] Maalej A, Abid Y, Kallel A, Daoud A, Lautie A and Romain F 1997 *Solid State Commun.* **103** 279
[52] Kawamura Y, Mashiyama H and Hasebe K 2002 *J. Phys. Soc. Jpn.* **71** 1694
[53] Even J, Pedesseau L, Jancu J and Katan C 2013 *J. Phys. Chem. Lett.* **4** 2999
[54] Giorgi G, Fujisawa J, Segawa H and Yamashita K 2013 *J. Phys. Chem. Lett.* **4** 4213
[55] Feng J, Xiao B, Chen J C, Zhou C T, Du Y P and Zhou R 2009 *Solid State Commun.* **149** 1569
[56] Feng J, Xiao B, Pan W, Jiang Y H and Zhou R 2013 *Appl. Phys. Lett.* **103** 013902